Spatiotemporal Vortex Pulses: Angular Momenta and Spin-Orbit Interaction

Konstantin Y. Bliokh
Theoretical Quantum Physics Laboratory, RIKEN Cluster for Pioneering Research, Wako-shi, Saitama 351-0198, Japan

(Received 7 February 2021; accepted 19 May 2021; published 16 June 2021)

Recently, spatiotemporal optical vortex pulses carrying a purely transverse intrinsic orbital angular momentum were generated experimentally [Optica **6**, 1547 (2019); Nat. Photonics **14**, 350 (2020)]. However, an accurate theoretical analysis of such states and their angular-momentum properties remains elusive. Here, we provide such analysis, including scalar and vector spatiotemporal Bessel-type solutions as well as description of their propagational, polarization, and angular-momentum properties. Most importantly, we calculate both local densities and integral values of the spin and orbital angular momenta, and predict observable spin-orbit interaction phenomena related to the coupling between the transverse spin and orbital angular momentum. Our analysis is readily extended to spatiotemporal vortex pulses of other natures (e.g., acoustic).

DOI: 10.1103/PhysRevLett.126.243601

Introduction.—Vortex beams carrying intrinsic orbital angular momentum (OAM) are widely studied and exploited in modern optics [1–7], acoustics [8–13], and electron microscopy [14–20]. They have found numerous applications in a variety of classical and quantum systems. Such beams are monochromatic, and their intrinsic OAM is produced by a screw phase dislocation (vortex) aligned with the beam axis [21,22]. Thus, this OAM is *longitudinal*, i.e., aligned with the mean momentum of the beam.

Recently, spatiotemporal analogs of vortex beams, spatiotemporal vortex pulses (STVPs), were predicted theoretically [23–25] and generated experimentally in optics [26–30]. Such states are essentially polychromatic, and they carry intrinsic OAM *transverse* (or, generally, tilted) with respect to the propagation direction of the pulse. This OAM is produced by an edge (or mixed edge-screw) phase dislocation [21,22]. It is anticipated that the STVPs and transverse intrinsic OAM can considerably extend functionality and applications of wave vortices. In particular, while monochromatic vortex beams are essentially 3D objects, STVPs can exist in 2D spatial geometry. In addition, they can produce temporal analogs of spatial phenomena known for monochromatic vortex beams (e.g., time delays instead of beam shifts).

Despite the very recent progress in the generation of STVPs [27–30], they still lack an accurate theoretical description, including consistent analysis of their angular-momentum and polarization properties. Indeed, despite numerous mentions of the OAM in Refs. [27–30], its value has not been obtained there. Instead, the topological number of the phase dislocation ℓ was used, which generically does not coincide with the normalized OAM value [2,31]. Furthermore, accurate calculations of the OAM are impossible without a full-vector description and separation of the spin and orbital parts of the total angular momentum [7,32–34].

In this Letter, we fill this gap by constructing simple Bessel-type solutions for STVPs. We describe their propagational dynamics including "temporal diffraction" [25,27], examine polarization properties, and calculate both local densities and integral values of the OAM and spin angular momentum (SAM) of such pulses. We show that the in-plane linear polarization inevitably produces a longitudinal field component and a nonzero transverse SAM density. This induces the spin-orbit interaction effects, known for monochromatic beams [32,35], such as observable polarization-dependent intensity distributions of STVPs. Importantly, an integral value of the transverse SAM vanishes, while the integral OAM is quantized as $\hbar\ell$ per photon only for circularly symmetric pulses with equal width and length. For *elliptical* STVPs with different width and length, which were used in experiments [27–30], the OAM value is larger than $\hbar\ell$ per photon.

Thus, our work provides the self-consistent full-vector description of optical STVPs. It also allows straightforward extension to analogous acoustic pulses.

Scalar Bessel-type solutions.—We first consider scalar waves and simplest analytical vortex-beam solutions: Bessel beams [32,36–40]. Monochromatic Bessel beams propagating along the z axis can be constructed as a superposition of plane waves with the same frequency $\omega = \omega_0$, wave vectors $\mathbf{k}$ distributed within a cone of polar angle $\theta = \theta_0$, and with an azimuthal phase difference $\ell\phi$ (ϕ is the azimuthal angle in $\mathbf{k}$ space) corresponding to a vortex of integer order ℓ, Fig. 1(a). In other words, the wave vectors form a circle in the $k_z = k_\parallel$ plane, with the center at $(0, 0, k_\parallel)$ and radius $k_\perp$, where $k_\parallel = k_0 \cos\theta_0$, $k_\perp = k_0 \sin\theta_0$, $k_0 = \omega_0/c$, and c is the speed of light. In real space, this superposition results in the scalar wave function $\psi(\mathbf{r}, t) \propto J_\ell(k_\perp r) \exp(ik_\parallel z + i\ell\varphi - i\omega_0 t)$, where (r, φ)

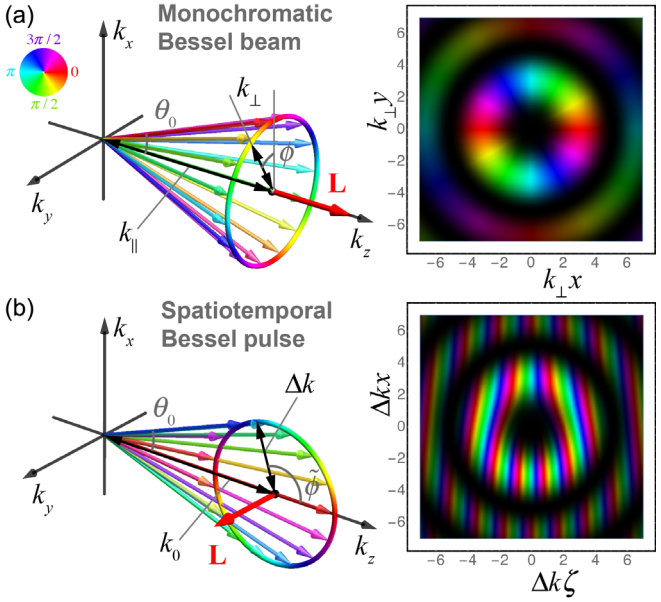

FIG. 1. The plane-wave spectra (left) and phase-intensity distributions of real-space wave functions $\psi(\mathbf{r},t)$ (right) for (a) the monochromatic Bessel beam with $\ell=2$ and (b) spatiotemporal Bessel pulse with $\ell=2$, Eqs. (1) and (2). In real-space distributions, the brightness is proportional to the intensity $|\psi|^2$, while the color indicates the phase $\mathrm{Arg}(\psi)$.

are the polar coordinates in the (x,y) plane and J_n is the Bessel function of the first kind. The transverse intensity and phase distributions of such Bessel beam are shown in Fig. 1(a).

To construct a Bessel-type STVP with a purely transverse intrinsic OAM, we use a superposition of plane waves with wave vectors distributed over a circle in the $k_y=0$ plane with the center at $(0,0,k_0)$ and radius Δk, Fig. 1(b). Using the azimuthal angle $\tilde{\phi}$ with respect to the center of this circle, we introduce the azimuthal phase difference $\ell\tilde{\phi}$ and write the real-space wave function as a Fourier-type integral:

$$\psi(\mathbf{r},t)\propto\int_0^{2\pi}e^{i[k_0z+\Delta k\cos\tilde{\phi}\,z+\Delta k\sin\tilde{\phi}\,x+\ell\tilde{\phi}-\omega(\tilde{\phi})t]}d\tilde{\phi},\qquad(1)$$

where $\omega(\tilde{\phi})=c\sqrt{k_0^2+\Delta k^2+2k_0\Delta k\cos\tilde{\phi}}$. Parameter Δk determines the degree of paraxiality and monochromaticity of the Bessel STVP. The maximum polar angle of the wave vectors in its spectrum is $\sin\theta_0=\Delta k/k_0$, Fig. 1(b). For $\Delta k\ll k_0$, $\theta_0\ll 1$, the pulse can be considered as near-paraxial and quasimonochromatic. Below, we will use this approximation keeping terms linear in θ_0, which describe some postparaxial phenomena.

In this approximation, $\omega(\tilde{\phi})\simeq c(k_0+\Delta k\cos\tilde{\phi})$, and the integral (1) results in the analytical Bessel-pulse solution:

$$\psi(\mathbf{r},t)\propto J_\ell(\tilde{\rho})\exp(ik_0\zeta+i\ell\tilde{\varphi}).\qquad(2)$$

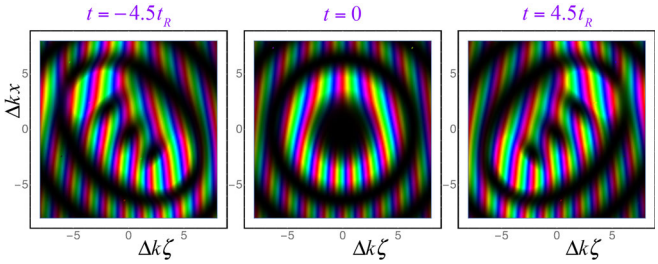

FIG. 2. Temporal diffraction of the spatiotemporal Bessel pulse (1) with $\ell=3$ and $\Delta k/k_0=0.3$. The characteristic timescale $ct_R=k_0/\Delta k^2$ is analogous to the Rayleigh range of spatially diffracting beams.

Here, $\zeta=z-ct=\tilde{r}\cos\tilde{\varphi}$, $\tilde{\rho}=\Delta k\tilde{r}$, and $(\tilde{r},\tilde{\varphi})$ are the polar coordinates in the (ζ,x) plane. The intensity $I=|\psi|^2$ and phase $\mathrm{Arg}(\psi)$ distributions for the Bessel STVP (2) are shown in Fig. 1(b). It has typical Bessel-beam intensity profile $I\propto|J_\ell(\tilde{\rho})|^2$ in the (ζ,x) plane, contains an edge phase dislocation of order ℓ, and propagates with the speed of light along the z axis.

Importantly, the nondiffracting solution (2) is a result of linear expansion of $\omega(\tilde{\phi})$ with respect to Δk. The exact solution (1) evolves in time as shown in Fig. 2. Namely, the ℓth order phase dislocation in the pulse center splits into a raw of $|\ell|$ first-order dislocations oriented diagonally in the (ζ,x) plane. This temporal diffraction was predicted in Ref. [25] and observed in [27]. Akin to the Rayleigh range characterizing spatial diffraction, a typical scale of the temporal diffraction is given by the "temporal Rayleigh range" $ct_R=k_0/\Delta k^2$, Fig. 2. Notably, nondiffracting Bessel-like STVPs can be constructed using the wave vectors distributed along an ellipse in $\mathbf{k}$ space which could be Lorentz transformed to a monochromatic circle [25]. In our case, the circular spectrum in Fig. 1(b) should be extended along the k_z axis to become an ellipse with the ratio of semiaxes $\gamma=\sqrt{1+(k_0/\Delta k)^2}$.

Vector solutions and spin-orbit effects.—We now examine vector Bessel STVPs. For simplicity, we consider the electric field $\mathbf{E}$ of transverse electromagnetic waves; similar arguments could be applied to the magnetic field and other types of vector waves. Because of the transversality condition, the electric field of each plane wave in the pulse spectrum must be orthogonal to its wave vector $\mathbf{k}$. This determines two basic polarizations in the problem: (i) out-of-plane, $\mathbf{E}$ is directed along the y axis, Fig. 3(a), and (ii) in-plane, $\mathbf{E}$ lies in the (z,x) plane, Fig. 3(b).

For the out-of-plane polarization, the field has only one component, and the problem reduces to the scalar case: $E_y(\mathbf{r},t)\propto\psi(\mathbf{r},t)$.

For the in-plane polarization, the situation is less trivial. Each plane wave in the pulse spectrum has two electric-field components, E_x and E_z, Fig. 3(b). The amplitudes and phases of these components depend on the wave vector $\mathbf{k}$, which signals the spin-orbit interaction [32,35]. To describe

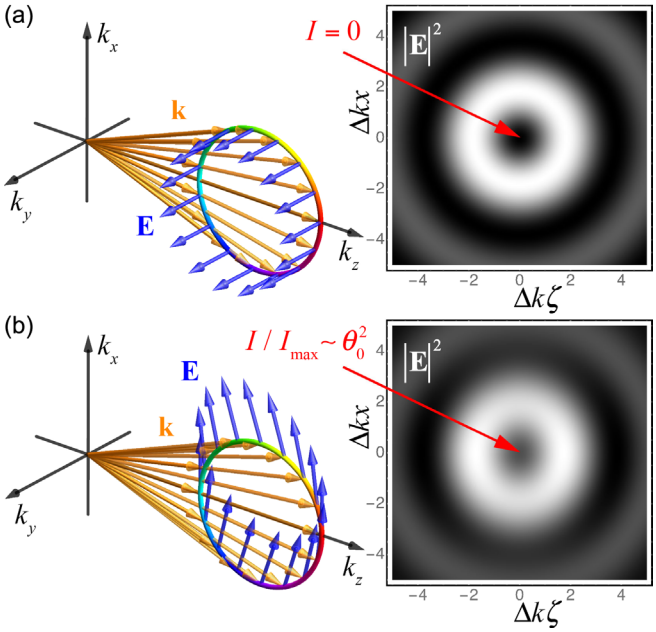

FIG. 3. Electric fields of plane waves in the spectra of Bessel-type vector STVPs (left) and the corresponding real-space intensity distributions $|\mathbf{E}(\mathbf{r},t)|^2$ (right) for (a) the out-of-plane polarization and (b) the in-plane polarization. The parameters are $\ell = 1$ and $\Delta k = 0.7$ for better visibility of nonzero intensity (5) in the center of the pulse in (b).

the spin-orbit effects in the linear approximation in Δk, we write the electric-field components for each plane wave as $E_x = E\cos\theta \simeq E$ and $E_z = -E\sin\theta \simeq -E(\Delta k/k_0)\sin\tilde{\phi}$, where $\theta \le \theta_0$ is the polar angle of a given wave vector. Since for the integrand of Eq. (1), $i\Delta k\sin\tilde{\phi} = \partial/\partial x$, one can write the real-space transverse (x) and longitudinal (z) field components as

$$E_x(\mathbf{r},t) \simeq \psi(\mathbf{r},t), \qquad E_z(\mathbf{r},t) \simeq \frac{i}{k_0}\frac{\partial\psi(\mathbf{r},t)}{\partial x}. \tag{3}$$

Substituting Eq. (2) into Eq. (3), we obtain the longitudinal field

$$E_z \propto \frac{i\Delta k}{2} e^{ik_0\zeta}[e^{i(\ell-1)\tilde{\varphi}}J_{\ell-1}(\tilde{\rho}) + e^{i(\ell+1)\tilde{\varphi}}J_{\ell+1}(\tilde{\rho})]. \tag{4}$$

From Eqs. (2)–(4), the total field intensity, $I = |E_x|^2 + |E_z|^2$, is given by

$$I \propto J_\ell^2 + \frac{\Delta k^2}{4k_0^2}[J_{\ell-1}^2 + J_{\ell+1}^2 + 2\cos(2\tilde{\varphi})J_{\ell-1}J_{\ell+1}]. \tag{5}$$

Here and hereafter, for brevity, we omit the Bessel-functions argument $\tilde{\rho}$.

The intensity distribution of the Bessel STVP, Eq. (5), resembles intensity distributions of vector Bessel beams in optics [32], acoustics [41], and quantum mechanics [42]. In particular, the presence of the Bessel functions of orders $\ell \pm 1$ is a typical signature of the spin-orbit interaction. The easiest-to-observe spin-orbit effect is a nonzero intensity $\sim\theta_0^2$ in the center of the in-plane-polarized STVPs with $|\ell| = 1$, Fig. 3. For monochromatic vortex beams, this phenomenon has been observed in optical experiments [35,43,44]. The main difference is that in the case of monochromatic vortex beams this effect occurs for *circular* polarizations, corresponding to the longitudinal SAM of the beam, while for STVPs it takes place for the in-plane *linear* polarization. As we show below, this polarization generates a nonzero transverse SAM density directed along the y axis, i.e., along with the intrinsic OAM of the pulse.

Spin and orbital angular momenta.—Analysis of the spin and orbital angular momenta of polychromatic STVPs is a challenging problem because most theoretical methods are developed for monochromatic fields. Indeed, standard formulas for the SAM and OAM densities imply averaging over the cycle of periodic temporal oscillations [7], and they become ill defined in generic polychromatic fields [34]. Nonetheless, here we can employ the quasimonochromaticity of pulses with $\Delta k \ll k_0$ and separate fast temporal oscillations with the central frequency $\omega_0 = k_0 c$ and slow temporal evolution with the inverse temporal scale Δkc. This results in the SAM and OAM densities given by the standard monochromatic formulas involving canonical SAM and OAM operators and time-dependent "wave function" $\mathbf{E}(\mathbf{r},t)e^{i\omega_0 t}/\sqrt{\omega_0}$ [7]:

$$S_y = \omega_0^{-1}\mathrm{Im}(\mathbf{E}^*\times\mathbf{E})_y, \qquad L_y = \omega_0^{-1}\mathrm{Im}\left(\mathbf{E}^*\cdot\frac{\partial}{\partial\tilde{\varphi}}\mathbf{E}\right). \tag{6}$$

Although the angle $\tilde{\varphi}$ in the (ζ, x) plane involves time, in Eq. (6) we used the fact that at $t = 0$ it becomes the desired azimuthal angle in the (z, x) plane, whereas in the diffractionless approximation the SAM and OAM distributions are invariantly translated together with the pulse along the z axis.

For the out-of-plane polarization (the scalar case), Eqs. (6) yield

$$S_y = 0, \qquad L_y = \omega_0^{-1}(\ell - k_0 x)I, \tag{7}$$

where $I \propto J_{|\ell|}^2(\tilde{\rho})$. The OAM density (7) contains the standard vortex-related term proportional to ℓ as well as the $k_0 x$-dependent term caused by the z propagation of the pulse. After integration of the OAM density L_y over the (z, x) plane, the $k_0 x$ term vanishes, while the vortex-induced term yields the integral value of $\hbar\ell$ per photon [1–7]: $\omega_0\langle L_y\rangle/\langle I\rangle = \ell$. Here, $\langle\cdots\rangle = \int\cdots dzdx = \int\cdots d\zeta dx$ and we imply quasimonochromatic quantization of photon's energy, $\hbar\omega_0$.

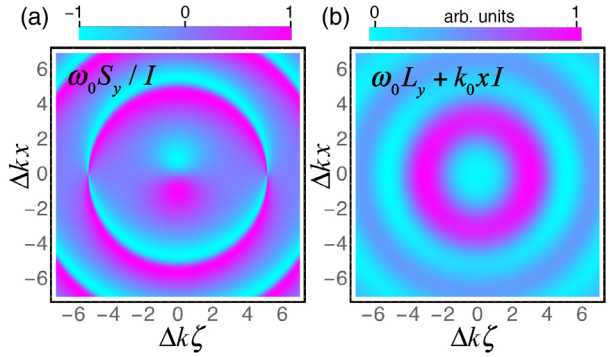

FIG. 4. Spatial distributions of (a) the normalized transverse spin angular momentum density $\omega_0 S_y / I$ and (b) the orbital angular momentum density (with the subtracted propagational term) $\omega_0 L_y + k_0 x I$ in the in-plane-polarized Bessel STVP, Eqs. (8) and (5). The parameters are $\ell = 2$ and $\Delta k / k_0 = 0.5$.

For the in-plane polarized pulse (3)–(5), Eqs. (6) yield

$$S_y \propto \omega_0^{-1} \frac{\Delta k^2 x}{2\ell k_0} (J^2_{\ell+1} - J^2_{\ell-1}),$$
$$L_y = \omega_0^{-1} (\ell - k_0 x) I + \frac{\ell}{2 k_0 x} S_y. \tag{8}$$

These distributions are depicted in Fig. 4. The nonzero spin density S_y is a manifestation of the transverse spin phenomenon, which recently attracted great attention [7,35,45–47]. Here, the transverse spin arises from the interference of plane waves with different directions, phases, and in-plane linear polarizations, Fig. 3(b). The normalized SAM density $\omega_0 S_y / I$ reaches the minimum and maximum values of -1 and 1, Fig. 4(a), i.e., the polarization becomes left-hand and right-hand circular in these zones. As is typical for the transverse spin of free-space propagating waves [7,45,47], its integral value vanishes: $\langle S_y \rangle = 0$.

The OAM density (8) has a form similar to Eq. (7) with an additional spin-related term; this is also a signature of the spin-orbit interaction [32,35]. Nonetheless, in contrast to the analogous spin-dependent OAM parts in monochromatic beams, the integral value of this term vanishes. [This follows from the relation $\ell \int_0^\infty (J^2_{\ell+1} - J^2_{\ell-1}) \tilde{\rho} d\tilde{\rho} \propto \ell \int_0^\infty J_\ell (dJ_\ell / d\tilde{\rho}) d\tilde{\rho} = 0$.] Thus, akin to the scalar case, the integral OAM value corresponds to $\hbar\ell$ per photon.

We conclude that in spite of local spin-orbit interaction effects, the integral SAM and OAM of STVPs are rather robust:

$$\langle S_y \rangle = 0, \qquad \frac{\omega_0 \langle L_y \rangle}{\langle I \rangle} = \ell. \tag{9}$$

Importantly, the above calculations are made for STVPs with *circularly* symmetric intensity profiles in the (ζ, x) plane. However, in most cases these profiles are *elliptical*

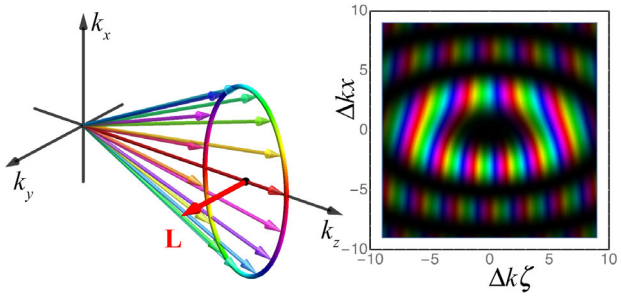

FIG. 5. The plane-wave spectrum (left) and the phase-intensity distribution of the real-space wave function $\psi(\mathbf{r}, t)$ (right) for an elliptical Bessel STVP with $\ell = 2$ and ratio of principal axes $\gamma = 2$. The normalized integral OAM of this pulse is $\omega_0 \langle L_y \rangle / \langle I \rangle = 2.5$, Eq. (10).

with some ratio of principal axes γ, as shown in Fig. 5. Such an elliptical STVP is described by the substitution $x \to \gamma x$ in the scalar wave function (1) and (2) or, equivalently, by the substitution $k_x \to \gamma^{-1} k_x$ in the beam spectrum. For the field of the form $\propto \exp(i\ell\tilde{\varphi})$ and the OAM operator $\hat{L}_y = -i\partial/\partial\tilde{\varphi} = i(x\partial/\partial\zeta - \zeta\partial/\partial x)$, this results in an additional factor in the intrinsic OAM value [25,48]:

$$\frac{\omega_0 \langle L_y \rangle}{\langle I \rangle} = \frac{\gamma + \gamma^{-1}}{2} \ell. \tag{10}$$

This factor is significant: for example, the experiments [27,28] generated STVPs with $\gamma \simeq 2.5$–3, which yields $(\gamma + \gamma^{-1})/2 \simeq 1.5$–1.7 Figure 5 shows an example of the STVPs with $\ell = 2$, $\gamma = 2$, and $\omega_0 \langle L_y \rangle / \langle I \rangle = 2.5$.

Conclusions.—We have examined spatiotemporal vortex pulses with purely transverse intrinsic orbital angular momentum. We provided analytical Bessel-type solutions, both scalar and vector, and described their propagation, polarization, and angular-momentum properties. Most importantly, we provided accurate calculations of the spin and orbital angular momenta of STVPs and described observable spin-orbit interaction phenomena. Notably, the polarization and spin-orbit effects manifest themselves locally via observable intensity and spin-density distributions, while the integral values of the spin and orbital angular momenta of STVPs are rather robust. At the same time, the integral OAM value is significantly affected by the elliptical shape of STVPs with different width and length, which are typically generated in experiments [27,28].

The results of our work provide a theoretical platform for investigations of novel spatiotemporal vortex states and call for experimental measurements of the predicted polarization and angular-momentum phenomena. We considered Bessel-type pulses solely for the simplicity of their theoretical description. The results can be straightforwardly generalized to the Laguerre-Gaussian-type spectra [1–4], more relevant to typical experimental situations. Furthermore, a variety of phenomena, well studied for

monochromatic vortex beams, can now be investigated for STVPs: e.g., fractional OAM [49,50], shifts at planar interfaces [51,52], etc.

Importantly, our results are applicable to waves of different natures. For example, STVPs can be generated in sound waves in fluids or gases. In doing so, one can use the scalar approach (1) and (2) for the pressure wave field $P(\mathbf{r},t)$ or the vector approach similar to Eqs. (3)–(5) for the velocity wave field $\mathbf{V}(\mathbf{r},t)$. Since sound waves are *longitudinal*, i.e., $\mathbf{V}\|\mathbf{k}$ for each plane wave in the spectrum, the velocity field has the z and x components, $V_z(\mathbf{r},t)\simeq\psi(\mathbf{r},t)$ and $V_x(\mathbf{r},t)\simeq -ik_0^{-1}\partial\psi(\mathbf{r},t)/\partial x$, generating the transverse spin and related spin-orbit phenomena [41,53].

[1] L. Allen, M. W. Beijersbergen, R. J. C. Spreeuw, and J. P. Woerdman, Orbital angular momentum of light and the transformation of Laguerre-Gaussian laser modes, Phys. Rev. A **45**, 8185 (1992).

[2] *Optical Angular Momentum*, edited by L. Allen, S. M. Barnett, and M. J. Padgett (Taylor and Francis, London, 2003).

[3] A. Bekshaev, M. Soskin, and M. Vasnetsov, *Paraxial Light Beams with Angular Momentum* (Nova Science Publishers, New York, 2008).

[4] *The Angular Momentum of Light*, edited by D. L. Andrews and M. Babiker (Cambridge University Press, Cambridge, England, 2012).

[5] G. Molina-Terriza, J. P. Torres, and L. Torner, Twisted photons, Nat. Phys. **3**, 305 (2007).

[6] S. Franke-Arnold, L. Allen, and M. J. Padgett, Advances in optical angular momentum, Laser Photonics Rev. **2**, 299 (2008).

[7] K. Y. Bliokh and F. Nori, Transverse and longitudinal angular momenta of light, Phys. Rep. **592**, 1 (2015).

[8] B. T. Hefner and P. L. Marston, An acoustical helicoidal wave transducer with applications for the alignment of ultrasonic and underwater systems, J. Acoust. Soc. Am. **106**, 3313 (1999).

[9] J. Lekner, Acoustic beams with angular momentum, J. Acoust. Soc. Am. **120**, 3475 (2006).

[10] K. Volke-Sepulveda, A. O. Santillan, and R. R. Boullosa, Transfer of Angular Momentum to Matter From Acoustical Vortices in Free Space, Phys. Rev. Lett. **100**, 024302 (2008).

[11] C. E. M. Demore, Z. Yang, A. Volovick, S. Cochran, M. P. MacDonald, and G. C. Spalding, Mechanical Evidence of the Orbital Angular Momentum to Energy Ratio of Vortex Beams, Phys. Rev. Lett. **108**, 194301 (2012).

[12] A. Anhauser, R. Wunenburger, and E. Brasselet, Acoustic Rotational Manipulation Using Orbital Angular Momentum Transfer, Phys. Rev. Lett. **109**, 034301 (2012).

[13] A. Marzo, M. Caleap, and B. W. Drinkwater, Acoustic Virtual Vortices with Tunable Orbital Angular Momentum for Trapping of Mie Particles, Phys. Rev. Lett. **120**, 044301 (2018).

[14] K. Y. Bliokh, Y. P. Bliokh, S. Savel'ev, and F. Nori, Semiclassical Dynamics of Electron Wave Packet States with Phase Vortices, Phys. Rev. Lett. **99**, 190404 (2007).

[15] M. Uchida and A. Tonomura, Generation of electron beams carrying orbital angular momentum, Nature (London) **464**, 737 (2010).

[16] J. Verbeeck, H. Tian, and P. Schattschneider, Production and application of electron vortex beams, Nature (London) **467**, 301 (2010).

[17] B. J. McMorran, A. Agrawal, I. M. Anderson, A. A. Herzing, H. J. Lezec, J. J. McClelland, and J. Unguris, Electron vortex beams with high quanta of orbital angular momentum, Science **331**, 192 (2011).

[18] K. Y. Bliokh, I. P. Ivanov, G. Guzzinati, L. Clark, R. Van Boxem, A. Beche, R. Juchtmans, M. A. Alonso, P. Schattschneider, F. Nori, and J. Verbeeck, Theory and applications of free-electron vortex states, Phys. Rep. **690**, 1 (2017).

[19] S. M. Lloyd, M. Babiker, G. Thirunavukkarasu, and J. Yuan, Electron vortices: Beams with orbital angular momentum, Rev. Mod. Phys. **89**, 035004 (2017).

[20] H. Larocque, I. Kaminer, V. Grillo, G. Leuchs, M. J. Padgett, R. W. Boyd, M. Segev, and E. Karimi, 'Twisted' electrons, Contemp. Phys. **59**, 126 (2018).

[21] J. F. Nye and M. V. Berry, Dislocations in wave trains, Proc. R. Soc. Ser. A **336**, 165 (1974).

[22] M. V. Berry, in *Les Houches Lecture Series Session XXXV* (North-Holland, Amsterdam, 1981), Chap. Singularities in Waves, pp. 453–543.

[23] A. P. Sukhorukov and V. V. Yangirova, Spatio-temporal vortices: Properties, generation and recording, Proc. SPIE Int. Soc. Opt. Eng. **5949**, 594906 (2005).

[24] N. Dror and B. A. Malomed, Symmetric and asymmetric solitons and vortices in linearly coupled two-dimensional waveguides with the cubic-quintic nonlinearity, Physica (Amsterdam) **240D**, 526 (2011).

[25] K. Y. Bliokh and F. Nori, Spatiotemporal vortex beams and angular momentum, Phys. Rev. A **86**, 033824 (2012).

[26] N. Jhajj, I. Larkin, E. W. Rosenthal, S. Zahedpour, J. K. Wahlstrand, and H. M. Milchberg, Spatiotemporal Optical Vortices, Phys. Rev. X **6**, 031037 (2016).

[27] S. W. Hancock, S. Zahedpour, A. Goffin, and H. M. Milchberg, Free-space propagation of spatiotemporal optical vortices, Optica **6**, 1547 (2019).

[28] A. Chong, C. Wan, J. Chen, and Q. Zhan, Generation of spatiotemporal optical vortices with controllable transverse orbital angular momentum, Nat. Photonics **14**, 350 (2020).

[29] S. W. Hancock, S. Zahedpour, and H. M. Milchberg, Second harmonic generation of spatiotemporal optical vortices and conservation of orbital angular momentum, Optica **8**, 594 (2021).

[30] C. Wan, J. Chen, A. Chong, and Q. Zhan, Experimental demonstration of ultrafast wavepacket containing orbital angular momentum with controllable orientation, arXiv: 2101.04949.

[31] M. V. Berry, Paraxial beams of spinning light, Proc. SPIE Int. Soc. Opt. Eng. **3487**, 6 (1998).

[32] K. Y. Bliokh, M. A. Alonso, E. A. Ostrovskaya, and A. Aiello, Angular momenta and spin-orbit interaction of

nonparaxial light in free space, Phys. Rev. A **82**, 063825 (2010).
[33] S. M. Barnett, Rotation of electromagnetic fields and the nature of optical angular momentum, J. Mod. Opt. **57**, 1339 (2010).
[34] I. Bialynicki-Birula and Z. Bialynicka-Birula, Canonical separation of angular momentum of light into its orbital and spin parts, J. Opt. **13**, 064014 (2011).
[35] K. Y. Bliokh, F. J. Rodríguez-Fortuño, F. Nori, and A. V. Zayats, Spin-orbit interactions of light, Nat. Photonics **9**, 796 (2015).
[36] J. Durnin, Exact solutions for nondiffracting beams. I. The scalar theory, J. Opt. Soc. Am. A **4**, 651 (1987).
[37] J. Durnin, J. J. Miceli, and J. H. Eberly, Diffraction-Free Beams, Phys. Rev. Lett. **58**, 1499 (1987).
[38] D. McGloin and K. Dholakia, Bessel beams: Diffraction in a new light, Contemp. Phys. **46**, 15 (2005).
[39] Z. Bouchal and M. Olivik, Non-diffractive vector Bessel beams, J. Mod. Opt. **42**, 1555 (1995).
[40] R. Jauregui and S. Hacyan, Quantum-mechanical properties of Bessel beams, Phys. Rev. A **71**, 033411 (2005).
[41] K. Y. Bliokh and F. Nori, Spin and orbital angular momenta of acoustic beams, Phys. Rev. B **99**, 174310 (2019).
[42] K. Y. Bliokh, M. R. Dennis, and F. Nori, Relativistic Electron Vortex Beams: Angular Momentum and Spin-Orbit Interaction, Phys. Rev. Lett. **107**, 174802 (2011).
[43] N. Bokor, Y. Iketaki, T. Watanabe, and M. Fujii, Investigation of polarization effects for high-numerical-aperture first-order Laguerre-Gaussian beams by 2D scanning with a single fluorescent microbead, Opt. Express **13**, 10440 (2005).
[44] Y. Gorodetski, A. Niv, V. Kleiner, and E. Hasman, Observation of the Spin-Based Plasmonic Effect in Nanoscale Structures, Phys. Rev. Lett. **101**, 043903 (2008).
[45] A. Aiello, P. Banzer, M. Neugebauer, and G. Leuchs, From transverse angular momentum to photonic wheels, Nat. Photonics **9**, 789 (2015).
[46] P. Lodahl, S. Mahmoodian, S. Stobbe, A. Rauschenbeutel, P. Schneeweiss, J. Volz, H. Pichler, and P. Zoller, Chiral quantum optics, Nature (London) **541**, 473 (2017).
[47] J. S. Eismann, L. H. Nicholls, D. J. Roth, M. A. Alonso, P. Banzera, F. J. Rodriguez-Fortuno, A. V. Zayats, F. Nori, and K. Y. Bliokh, Transverse spinning of unpolarized light, Nat. Photonics **15**, 156 (2021).
[48] K. Y. Bliokh and F. Nori, Relativistic Hall Effect, Phys. Rev. Lett. **108**, 120403 (2012).
[49] M. V. Berry, Optical vortices evolving from helicoidal integer and fractional phase steps, J. Opt. A **6**, 259 (2004).
[50] J. Leach, E. Yao, and M. J. Padgett, Observation of the vortex structure of a non-integer vortex beam, New J. Phys. **6**, 71 (2004).
[51] K. Y. Bliokh, I. V. Shadrivov, and Y. S. Kivshar, Goos-Hänchen and Imbert-Fedorov shifts of polarized vortex beams, Opt. Lett. **34**, 389 (2009).
[52] M. Merano, N. Hermosa, J. P. Woerdman, and A. Aiello, How orbital angular momentum affects beam shifts in optical reflection, Phys. Rev. A **82**, 023817 (2010).
[53] C. Shi, R. Zhao, Y. Long, S. Yang, Y. Wang, H. Chen, J. Ren, and X. Zhang, Observation of acoustic spin, Natl. Sci. Rev. **6**, 707 (2019).